

# MAPPING TECHNIQUE FOR STELLARATORS WITH REALISTIC MAGNETIC FIELD\*

Sergei V. Kasilov<sup>1</sup>, Winfried Kernbichler<sup>2</sup>, Viktor V. Nemov<sup>1</sup>, Martin F. Heyn<sup>2</sup>

<sup>1</sup>Institute of Plasma Physics, National Science Center “Kharkov Institute of Physics and Technology”, Ul. Akademicheskaya 1, 61108 Kharkov, Ukraine

<sup>2</sup>Institut für Theoretische Physik, Technische Universität Graz,  
Petersgasse 16, A-8010 Graz, Austria

## 1. Introduction

A Monte-Carlo (MC) method to solve the drift kinetic equation using the stochastic mapping technique has been proposed in Ref. [1]. A numerical implementation of this approach has been presented in Ref. [2]. However, two major simplifications were made, namely the use of a simplified stellarator magnetic field configuration allowing for only one minimum value of the magnetic field module within one toroidal field period and the neglect of the quasi-static radial electric field. In the present report, a more realistic stellarator field, namely that of W7-AS [3], is considered. In addition, also the effect of the radial electric field is implemented.

## 2. Mapping technique

Within the stochastic mapping approach, test particle orbits are traced only on those surfaces where the magnetic field module reaches a minimum along the magnetic field line, the minimum-B cuts. The full test particle orbit integration needed for the MC procedure is replaced by mapping of particle positions and velocities between minimum-B cuts. In this way, the integration procedure is speeded up, because the information about the respective particle dynamics is precomputed and stored. In a general case the topology of minimum-B cuts in realistic magnetic field geometry is rather complex. They have to be subdivided into a few regions with simpler topology (see Figs. 1 and 2). The convenient numbering of these regions can be performed with the help of a 2-D vector index  $\mathbf{m} = (n, m)$ , where  $n$  numbers magnetic field periods and  $m$  numbers the cuts within a single period,  $\varphi_n < \varphi < \varphi_{n+1}$ , where  $\varphi$  is the toroidal angle. The problem is simplified by employing a local set of magnetic coordinates  $x^i$  (see [2,4]) in each magnetic field period. Two of these coordinates satisfy the magnetic differential equation,  $\mathbf{B} \cdot \nabla x^i = 0$ ,  $i = 1, 2$ , where  $\mathbf{B}$  is the magnetic field, and the boundary conditions on the “reference cuts”  $\varphi = \varphi_n$ ,  $x^1 = R$ ,  $x^2 = Z$ , where  $(R, \varphi, Z)$  are cylindrical coordinates. The third coordinate is  $x^3 = \varphi - \varphi_{(n)}$ . Together with the period index  $n$  (discrete toroidal coordinate) these coordinates describe the particle position in space uniquely. When a test particle travels to one of the neighboring periods the change of the local coordinate

---

\*This work has been carried out within the Association EURATOM-ÖAW and under contract P13495-TPH with the Austrian Science Foundation.

system is accomplished with high accuracy with the help of the interpolated mapping procedure using bi-cubic splines.

Introducing the coordinates  $\mathbf{u}$  of footprints of test particle orbits on a minimum-B cut  $\mathbf{m}$ , where  $u^1 = x^1$ ,  $u^2 = x^2$ ,  $u^3 = p$ , and  $u^4 = \lambda$ , yields a unique set of footprint coordinates,  $(\mathbf{m}, \mathbf{u})$ . Without collisions, each new footprint of a drift orbit,  $(\mathbf{m}', \mathbf{u}')$ , is determined by the Poincaré map,  $\mathbf{m}' = \mathbf{M}_{\mathbf{m}}(\mathbf{u})$ ,  $u'^i = U_{\mathbf{m}}^i(\mathbf{u})$ , where  $\mathbf{M}_{\mathbf{m}}(\mathbf{u})$  gives the index of the next cut to be passed by the drift orbit. This can be one of two neighboring cuts, then such particle is called “passing”, or the same cut for a “trapped” one. The spatial components of the map can be expressed in terms of the particle displacement from the magnetic field line  $\Delta x_{\mathbf{m}}^{1,2}(\mathbf{u})$  with,  $U_{\mathbf{m}}^i(\mathbf{u}) = u^i + \Delta x_{\mathbf{m}}^i(\mathbf{u})$ . The displacements are well represented by expansion over the normalized momentum module  $\rho_B = p/(m\omega_c)$ , the radial electric field amplitude  $\rho_E = 2e\Phi'(\psi)/(p\omega_c)$ , and its derivative,  $\rho_E' = 2e\Phi''(\psi)/(p\omega_c)$ , as

$$\begin{aligned} \Delta x_{\mathbf{m}}^i &= \left( \frac{\partial \Delta x_{\mathbf{m}}^i}{\partial \rho_E} \right)_0 \rho_E + \left( \frac{\partial \Delta x_{\mathbf{m}}^i}{\partial \rho_B} \right)_0 \rho_B + \left( \frac{\partial^2 \Delta x_{\mathbf{m}}^i}{\partial \rho_B \partial \rho_{EE}} \right)_0 \rho_B \rho_{EE} + \\ &+ \frac{1}{2} \left( \frac{\partial^2 \Delta x_{\mathbf{m}}^i}{\partial \rho_B^2} \right)_0 \rho_B^2 + \left( \frac{\partial^2 \Delta x_{\mathbf{m}}^i}{\partial \rho_B \partial \rho_E} \right)_0 \rho_B \rho_E + \frac{1}{2} \left( \frac{\partial^2 \Delta x_{\mathbf{m}}^i}{\partial \rho_E^2} \right)_0 \rho_E^2, \end{aligned} \quad (1)$$

where  $\Phi$  is the electric potential and  $\psi$  is a flux surface label. Such an expansion reduces the problem of the map storage from 4-D to 3-D (only the  $\lambda$  dependence in velocity space remains non-trivial, see Fig. 3) and permits the use of different electric field profiles without reloading the orbits. The components of the map in the velocity space  $U_{\mathbf{m}}^3$  and  $U_{\mathbf{m}}^4$  need no storage because this mapping is performed with the help of conservation of energy and magnetic moment.

The account of diffusion in velocity space (Coulomb collisions) is realized by adding small random displacements  $\delta u_{\mathbf{m}}(\mathbf{u})$  to the regular map,  $\mathbf{m}' = \mathbf{M}_{\mathbf{m}}(\mathbf{u} + \delta \mathbf{u}_{\mathbf{m}}(\mathbf{u}))$ ,  $u'^i = U_{\mathbf{m}}^i(\mathbf{u} + \delta \mathbf{u}_{\mathbf{m}}(\mathbf{u}))$  thus making it stochastic. In the long-mean-free-path regime being of interest here, only the variance and deviation of these random displacements have to fulfil the relations  $\langle \delta u^i \rangle = \mathcal{F}_{\mathbf{m}}^i(\mathbf{u})$  and  $\langle \delta u^i \delta u^j \rangle = 2\bar{D}_{\mathbf{m}}^{ij}(\mathbf{u})$ , where  $\bar{D}_{\mathbf{m}}^{ij}$  and  $\mathcal{F}_{\mathbf{m}}^i$  are orbit integrated components of the diffusion tensor and the drag force [1,2]. In case of Coulomb collisions the dependence of these quantities on  $u^3 = p$  can also be factorized, and the main care has to be taken to reconstruct the dependence on the pitch (Fig. 4).

### 3. Results of benchmarking

In the present report the stochastic mapping technique has been benchmarked against the conventional MC method in regimes with and without electric field and against the field-line integration method [5] for evaluating transport coefficients in  $1/\nu$  regime. For both MC procedures a simplified Lorentz collision operator describing only pitch-angle scattering has been used. The long-mean-free-path regime has been considered with

$L_c/l = 0.003$  where  $L_c = 2\pi R/l$  and  $l = v/\nu_\perp$  are the connection length and the mean-free path, resp.. Here  $\nu_\perp$  is a perpendicular scattering frequency. The computed diffusion coefficient has been normalized to the mono-energetic plateau diffusion coefficient,  $D_\perp^{\text{plateau}} = \pi\rho_L^2 v/(16lR)$ , where  $\rho_L$  is the gyro-radius. The radial electric field profile was chosen to keep the electric rotation frequency  $\omega_E = c(d\Phi/dr)/(rB)$  close to constant along the small radius  $r$ . For benchmarking with the field line integration technique the “effective ripple amplitude”  $\epsilon_{\text{eff}}^{3/2}$  has been calculated. For an arbitrary stellarator, this quantity is substituted for the helical ripple amplitude  $\epsilon_h$  in formulas for  $1/\nu$  transport coefficients for the standard stellarator. The results stay in good agreement (Figs. 5, 6).

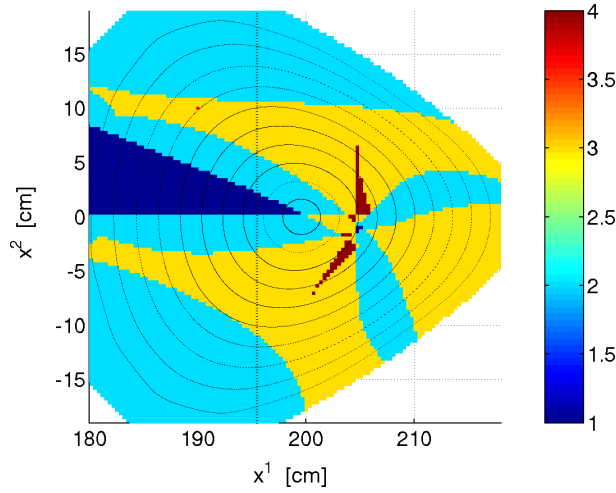


Fig. 1. Number of cuts within the magnetic field period in local magnetic coordinates  $x^i$ .

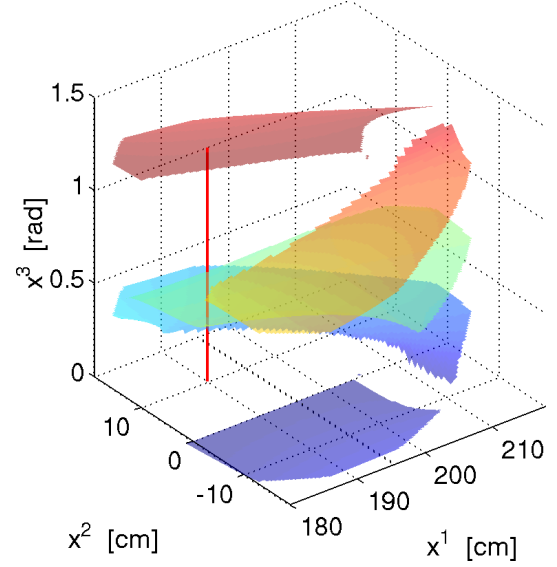


Fig. 2. The geometry of minimum-B cuts.

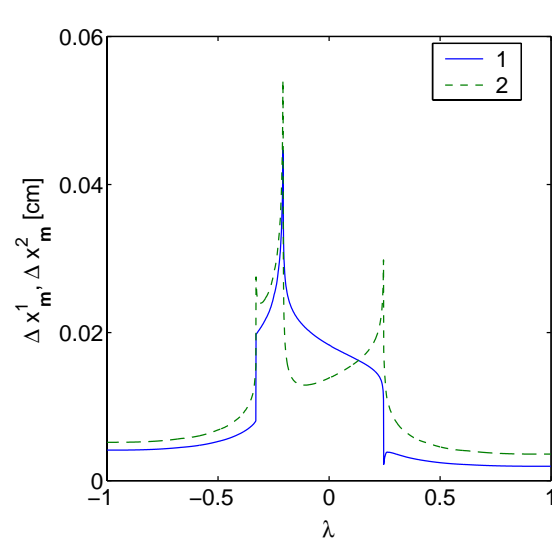


Fig. 3. Particle displacements  $\Delta x_{\mathbf{m}}^i$  as functions of the pitch  $\lambda$ .

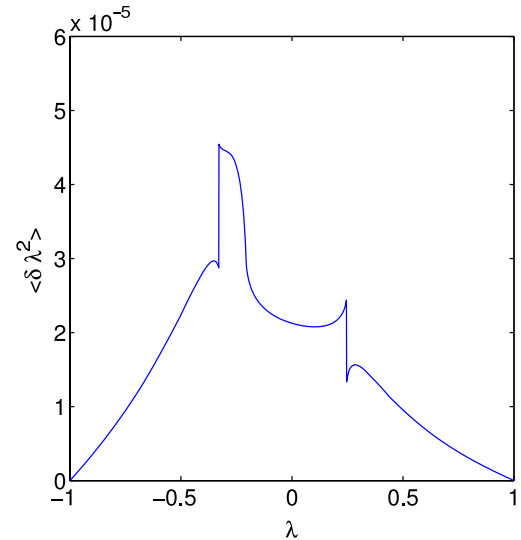


Fig. 4. Variance of the pitch per bounce time,  $\langle \delta\lambda^2 \rangle = 2\bar{D}_{\mathbf{m}}^{\lambda\lambda}$ , as a function of the pitch  $\lambda$ .

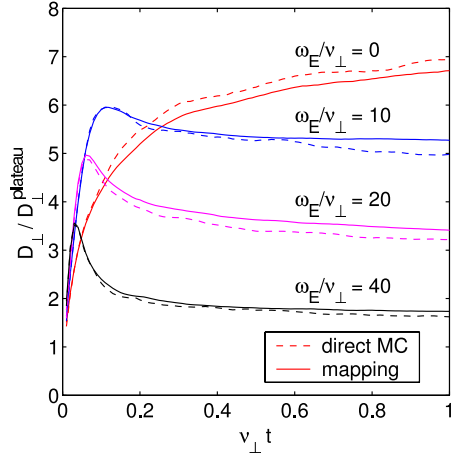


Fig. 5. Diffusion coefficient  $D_{\perp} = \langle \Delta r^2 / (2t) \rangle$  in units of the plateau coefficient versus relaxation time  $t$  for different values of the radial electric field. Starting point  $x^1 = 204$  cm,  $x^2 = -5.1$  cm.

#### 4. Discussion

The stochastic mapping technique has been developed and realized in a numerical code for the solution of the drift kinetic equation in a stellarator with arbitrary geometry and topology of the magnetic field, allowing for islands and ergodic magnetic field layers. The regimes with radial electric field in case of a simple magnetic field topology are well reproduced as compared to the conventional MC method. On the other hand, the mapping procedure is significantly faster (160 times in the considered case). Note that the speed of the mapping solver is practically independent of the complexity and computational cost of the magnetic field, therefore, the gain will be even more significant for configurations with a broad magnetic field spectrum. Since the preloading procedure is relatively time consuming, the method is most effective in a case when "global" computations of the particle distribution function are needed, e.g. for the studies of kinetic effects of rf-heating, or for the computation of profiles of transport coefficients for fixed magnetic configurations.

#### References

- [1] S.V. Kasilov, V.E. Moiseenko, and M.F. Heyn, *Phys. Plasmas*, **4** (1997) 2422.
- [2] S.V. Kasilov, W. Kernbichler, V.V. Nemov, and M.F. Heyn, *26<sup>th</sup> EPS Conf. on Contr. Fusion and Plasma Physics*, Maastricht, ECA **23J** (1999) 1629.
- [3] W. Dommaschk, W. Lotz, J. Nuehrenberg, *Nucl.Fusion* **24** (1984) 794.
- [4] A.M. Runov, D. Reiter, S.V. Kasilov, M.F. Heyn, and W. Kernbichler, *Phys. Plasmas*, **8** (2001) 916.
- [5] V.V. Nemov, S.V. Kasilov, W. Kernbichler, and M.F. Heyn, *Phys. Plasmas*, **6** (1999) 4622.

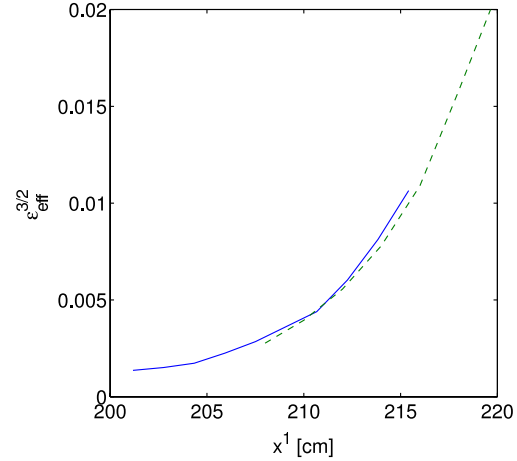


Fig. 6. Effective ripple amplitude  $\epsilon_{\text{eff}}^{3/2}$  as given by mapping (solid) and field line integration (dashed) techniques, respectively.